8-25-2014

Applying Accelerator Mass Spectrometry for Low-Level Detection of Complex Engineered Nanoparticles in Biological Media

Binghui Wang
University of Kentucky, binghui.wang@uky.edu

George S. Jackson
Purdue University

Robert A. Yokel
University of Kentucky, ryokel@email.uky.edu

Eric A. Grulke
University of Kentucky, eric.grulke@uky.edu

Applying Accelerator Mass Spectrometry for Low-Level Detection of Complex Engineered Nanoparticles in Biological Media

Applying accelerator mass spectrometry for low-level detection of complex engineered nanoparticles in biological media

Binghui Wang[1], George S. Jackson[2], Robert A. Yokel[3], Eric A. Grulke[1,]*

[1]Departments of Chemical and Materials Engineering, University of Kentucky, Lexington, KY 40506, [2]Purdue Rare Isotope Measurement Laboratory, Department of Physics, Purdue University, West Lafayette, IN, 47907, [3]Department of Pharmaceutical Sciences, University of Kentucky, Lexington, KY 40536. * Corresponding author: e-mail: eric.grulke@uky.edu. Tel.: +1 8592676097

Abstract

Complex engineered nanoparticles (CENPs), which have different core and surface components, are being developed for medicinal, pharmaceutical and industrial applications. One of the key challenges for environmental health and safety assessments of CENPs is to identify and quantity their transformations in biological environments. This study reports the effects of *in vivo* exposure of citrate-coated nanoalumina with different rare isotope labels on each component. This CENP was dosed to the rat and accelerator mass spectrometry (AMS) was used to quantify ^{26}Al, ^{14}C, and their ratio in the dosing material and tissue samples. For CENPs detected in the liver, the rare isotope ratio, ^{14}C/^{26}Al, was 87% of the dosing material's ratio. The citrate coating on the nanoalumina in the liver was stable or, if it degraded, its metabolites were incorporated with nearby tissues. However, in brain and bone where little alumina was detected, the rare isotope ratio greatly exceeded that of the dosing material. Therefore, in the animal, citrate dissociated from CENPs and redistributed to brain and bone. Tracking both the core and surface components by AMS presents a new approach for characterizing transformations of CENP components in biological milieu or environments.

Highlights

- The core and coating components of engineered nanoparticles were labeled with rare isotopes.
- These complex nanoparticles were injected into the rat.
- Dose and tissue samples were analyzed for both rare isotopes.
- The rare isotope ratio ($^{14}C/^{26}Al$) demonstrated the relative stability of the two CENP components

Keywords

complex engineered nanoparticles, nanoalumina, accelerator mass spectrometry, biodistribution

1. Introduction

Complex engineered nanoparticles are being developed for a variety of applications such as biomacromolecule receptors [1], biosensors [2], imaging indicators [3] and drug carriers [4]. The core nanoparticles include the metal oxides, such as alumina (Al_2O_3) [5]; ceria (CeO_2) [6, 7]; titania (TiO_2) [8]; zirconia (ZrO_2) [9]; and carbon-based nanomaterials, such as non-functionalized graphene [10, 11], single, and multi-walled carbon nanotubes [10, 12]. These core materials have extremely low aqueous solubility and therefore persist in biological media with potential to cause delayed toxicity [13-16]. In previous studies, we have found that, in the rat, a single intravenous administration of 30 nm ceria engineered nanoparticles distributed to specific organs within 24 hours; the ceria levels in these organs did not significantly decrease up to 90 days [17]. The coating materials, such as organic acids, silane coupling agents, proteins, or polymers, can control the dispersion and agglomeration of nanoparticles in fluids; they can also interact with solids and solutes in organisms and in the environment [11, 18, 19]. Citric acid, a tridentate carboxylic acid, has been widely applied on stabilizing metal oxide nanoparticles [20, 21]. The

fate of the citrate coating on these nanoparticles was not known. Therefore, the fate and toxicology of CENPs in biological media depends not only on the physico-chemical attributes of the core nanoparticle (size, size distribution, shape), but also their surface-bound molecular coatings. Material balances need to be performed on both the core and coatings materials in order to properly interpret their transport and transformations over the product life cycle.

The common characterization methods for bio-distribution and bio-persistence of CENPs are high-resolution transmission electron microscopy (HR-TEM) [22] and inductively coupled plasma mass spectrometry (ICP-MS) [23, 24]. The former can give good morphology information but may not provide sufficient chemical analysis. The latter provides good inorganic chemistry information but may not provide sufficient analysis of organic components. Some methods based on radioactive isotopes have been proposed. Perez-Campana et al. [25] utilized ^{13}N-labeled nanoalumina formed by proton beam activation to show bio-distribution in different organs. It verified that nanoalumina accumulated in the liver. As the half-life of ^{13}N is 9.97 min, it is useful for short time periods only. Rojas et al. [26] used the ^{18}F isotope to label the amino coating on ceria nanoparticles and showed that ceria accumulated mainly in lungs, spleen, and liver. However, labeling only one component of CENPs is not enough; the components might differentially dissociate, degrade, or transport in biological media.

Therefore, we used one isotope tracer for the core material and another for the coating material. Accelerator mass spectrometry (AMS), the most sensitive form of isotope ratio mass spectrometry, was used to characterize the two tracers. The AMS ion source produced negatively charged cesium ions to sputter the surface atoms of samples. A beam of negative ions, some of which were the radioactive tracer, were produced, and then accelerated to very high speed in a tandem accelerator. At the positive terminal of the tandem accelerator, the negative ions will undergo recharging to positive via a gas or carbon foil electron stripper,. Almost all molecular ions were dissociated in the procedure, since a beam with a positive charge of 4 or greater is typically selected (i.e. at least 5 electrons are removed) and molecular

ions dissociate. The ions of the rare isotope were easily selected using electric and magnetic fields and counted using nuclear detection techniques. One of the abundant stable isotopes is measured on the high energy side of the accelerator (after destruction of interfering molecular isobars) in a faraday cup and this provides the second part of the ratio (oftentimes denoted as rare/stable) [27, 28]. Therefore, this analysis tool can separate rare isotopes with high selectivity and sensitivity, detecting such species at levels 10^3 to 10^9 times lower than other methods [29, 30]. It has been applied in pharmaceutical and toxicological studies to investigate metabolism of drugs [31], covalent bonding of metabolite to RNA/ protein [32] and imaging of radioactive label [33, 34].

[This is not a complete sentence]Using AMS techniques to find and quantity low levels of complex nanoparticle components in biological systems where transporting or transformations might take place. Moreover, it should be possible to identify changes in the molar ratio (coating:core) after biological exposures of CENPs. Dual tracer technology should provide an understanding of the biodistribution and transformation of CENPs in various milieus. In this study, nanoalumina was used as the core material. It has very low solubility in aqueous systems and is relatively common in the environment; it has potential to enter biological tissue and persist there. The nanoalumina was synthesized using a hydrothermal system. ^{26}Al was introduced in the synthesis as the core material tracer. Hydroxyl groups on the nanoalumina surface can react with ^{14}C-labeled citric acid, used as a coating material. The citric acid was either covalently bound to the nanoparticle or self-crosslinked on the surface. The CENP, ^{26}Al-labeled nanoalumina core with ^{14}C-labeled coating, was infused into rats. The dosing material and selected tissues were analyzed by AMS in Purdue Rare Isotope Measurement Laboratory (PRIME lab) to quantify ^{26}Al and ^{14}C.

2. Experiments

2.1 Synthesis of neat nanoalumina

The synthesis route was modified from Chuah's work [35]. 0.001 mol of anhydrous aluminum chloride ($AlCl_3$, Acros) was dissolved in 10 mL 1 M HCl solution to form 0.1 mol/L $AlCl_3$ solution. Anhydrous $AlCl_3$ has a very high tendency to hydrolyze so it was dissolved in an acidic solution at a pH of about 2.5 to avoid precipitation. 1 mL ^{26}Al-HCl solution (16.5 nCi/mL, provided by the PRIME Lab) was diluted 10-fold. 600 μL of the diluted solution (1 nCi ^{26}Al) was added to the $AlCl_3$ solution. 0.5 M NaOH solution was added dropwise into the aluminum chloride solution with stirring until the pH was 9.5. AlO(OH) and $Al(OH)_3$ are formed in the process (scheme 1).

$$AlCl_3 + 3NaOH \rightarrow AlO(OH) + 3NaCl + H_2O$$

$$AlCl_3 + 3NaOH \rightarrow Al(OH)_3 + 3NaCl \qquad \text{Scheme 1}$$

The obtained white opaque mixtures were transferred to PTFE containers. The containers were inserted into a metal container (Parr Instrument Company, Models 4746). They were put in a furnace at 190 °C for 24 h, and then cooled to room temperature. The products were washed with distilled water three times and ultracentrifuged to remove the remaining Al^{3+} ion. The solid samples were dried at 90°C for 2 h to remove the adsorbed water and then heated to 600°C for ½ h. The AlO(OH) and $Al(OH)_3$ nanoparticles decomposed to form γ-alumina nanoparticles via calcination (scheme 2) [36].

$$2AlO(OH) \rightarrow Al_2O_3 + H_2O$$

$$2Al(OH)_3 \rightarrow Al_2O_3 + 3H_2O \qquad \text{Scheme 2}$$

The final samples were named "neat nanoalumina". The weight was 40 mg, 80% of the expected product mass. The expected radioactivity was ^{26}Al 0.02 nCi/mg.

2.2 Formation of citrate-coated nanoalumina

For coating nanoalumina with citric acid, 400 mg citric acid (MW=192, citric acid: alumina=10:1 w/w) was dissolved in 4 mL water. 50 μL citric acid with ^{14}C (0.05 mCi/mL, Amersham Bioscience UK limited, CFA263) was diluted into 5 mL, to 0.5 μCi/mL. 500 μL of this diluted solution (250 nCi ^{14}C) was added to the citric acid solution. Thermo-gravimetrical analysis showed that the adsorbed citric acid was 0.32% of that added. The adsorbed ^{14}C citric acid should have 0.8 nCi if the adsorbed/total ratio didn't change. 40 mg of neat nanoalumina was added to the citric acid solution, then the mixture was stirred for 24 h. The sample was washed by distilled water, ultracentrifuged and recovered three times to remove the free citric acid, and then was dried at 90 °C for 2 h. The dried sample was named "citrate-coated nanoalumina" with an expected radioactivity of 0.02 nCi/mg.

2.3 Characterization of nanoalumina

The shape and morphology of neat nanoalumina were observed by scanning electron microscopy (SEM, Hitachi 4300, University of Kentucky). Quantitation of hydroxyl and citrate groups on the surfaces of neat and citrated-coated nanoalumina was done via thermo gravimetric analysis (TGA) (Perkin Elmer, TGA-7 Thermo gravimetric Analyzer). In a nitrogen environment, the neat and citrate-coated nanoalumina were heated from room temperature to 110 °C, kept at 110 °C for ½ h to remove physically-adsorbed water, then heated to 750 °C at a rate of 10 °C/min. Within the higher temperature range, hydroxyl groups at the metal oxide surface will dehydrate to form water and the citrate coating will decompose to form carbon dioxide and ethylene [37]. To analyze the ability of citrate coating to create astable dispersion, some neat and citrate-coated nanoaluminas were dispersed in water with ultrasonication. The particle distribution in the dispersion was measured by dynamic light scattering (90 Plus, particle size analyzer, Brookhaven Instrument Corporation).

2.4 Animal infusions

20 mg of the citrate-coated nanoalumina was put into 1 ml water then ultrasonicated; the dispersion was expected to have 0.4 nCi ^{26}Al and 0.4 nCi ^{14}C/ml. One rat was intravenously infused, via a cannula inserted into a femoral vein that terminated in the vena cava, with 0.4 ml of this dispersion (anticipated dose 0.16 nCi ^{26}Al and 0.16 nCi ^{14}C). The dosed animal was terminated 30 days later and tissues, including liver, brain, and bone, were collected. The similar tissues from one un-dosed rat were collected as the control samples.

2.5 Sample preparation and AMS quantification of ^{26}Al

The pathways to analyze ^{26}Al and ^{14}C are described in the following paragraphs and summarized in Scheme-3 and Scheme-4.

To quantify ^{26}Al in the dosing material, it was diluted 100-fold to form a 0.2 mg/mL dispersion. 400 μL of the commercial analytical standard Al in HCl solution (Aluminum Standard for ICP, 10,000 mg/L in 5% nitric acid, 41377 Fluka) was added to two 10 μL aliquots of the diluted dosing material (Al_2O_3-1 and Al_2O_3-2). This enabled determination of the ^{26}Al/^{27}Al ratio by introducing a known amount of ^{27}Al (4 mg) that greatly exceeded the ^{27}Al in the sample. This was done to provide enough material for the AMS measurement. The two samples were then dried and ashed at 1000 °C.

To quantify ^{26}Al in tissue samples, each sample (from the dosed and control animals) was transferred to a scrupulously cleaned, pre-weighed, 7-ml Teflon screw-cap container and re-weighed to obtain sample weight. Four mg of ^{27}Al from the standard HCl solution was added to each sample. The mixture was dried at 110 °C. 3 ml 2:1 v/v mixture of HNO and H_2O_2 was added to digest the samples. After evaporating the liquid using a heatable, semi-closed system [38], the samples (except brain samples) were ashed at 1000 °C. For brain samples, direct ashing will result in some glasslike material believed to be aluminum oxyphosphate. A procedure that separates Al from phosphate was used [39]. A diluted mixture of HNO_3 and H_2O_2 was used to solubilize the residue after evaporating the liquid. Two grams of cation exchange

158 resin containing a sulfonic acid functional group (AG 50-X8, 100-200 mesh; Bio-Rad) was used to
159 complex the Al^{3+}. After washing three times with 5 mL 0.2% HNO_3, 5 mL of 1M hydrofluoric acid (HF)
160 was used to elute Al from the resin. The solution was dried by evaporation then ashed at 1000 °C. The
161 dosing material and tissue samples were sent to the PRIME lab for ^{26}Al quantification by AMS. Upon
162 receipt at the PRIME Lab, the samples were mixed with Ag in an approximately 2:1, Ag:Al_2O_3 weight
163 ratio. After mixing, the sample was inserted into a cavity in a sample holder (cathode) that was 0.040" in
164 diameter and 0.080" deep. The silver greatly increases the current out of the cesium sputter source and
165 increases efficiency of the measurement. The cathode was inserted into the PRIME Lab ion source. A
166 typical sample will produce a current of 500 nA in the source which translates to a count rate of
167 approximately 25 counts per minute for a sample with a $^{26}Al/^{27}Al$ ratio of 10^{-12}. Standards of known value
168 were measured before and after the assay of the unknowns and were used to normalize the ratios. Samples
169 were typically measured until they were used up or a precision of 3% was achieved.

170

171 2.6 Sample preparation and AMS quantification of ^{14}C

172 To quantify ^{14}C in the dosing material, it was diluted 10-fold to form a 2 mg/mL dispersion. Three 10 µL
173 aliquots of the diluted dispersion were collected (CA-1, CA-2 and CA-3). The CA 1-3 samples were sent
174 to the PRIME lab. For the dose material dilutions, tributyrin was added directly to the sample. Tributyrin
175 has no vapor pressure to speak of and is carbon rich. The $^{14}C:^{12}C$ ratio of the tributyrin is almost exactly 5
176 x 10^{-14}. The mixture was placed in a small quartz tube that was nestled in a Pyrex tube with a glass
177 microfiber filter in the top. The Pyrex tube was then placed in a centrifuge tube with another glass
178 microfiber filter in the top. The lid of the centrifuge tube had a few small holes drilled for water vapor
179 removal. This apparatus was then placed in a centrifuge and spun under vacuum for 24 h to remove the
180 water. The sample was then placed in a combustion tube with appropriate reactants, pumped to less than

15 microns as recorded by a gauge on the vacuum line. The tube was sealed with a torch, and placed in an oven to be combusted. The CO_2 was then transferred to another tube and graphitized using the method developed by Ognibene et.al [40].

The tributyrin method was good for the dosing material, since it had a very low content of carbon material. There was not enough material for an accurate AMS measurement without addition of a carrier. However, the tissue samples provide sufficient carbon content to permit direct measurements of the $^{14}C/^{12}C$ ratio without addition of a carrier. The tissue sample was located in a combustion tube with appropriate reactants, the tube sealed with a torch, and the contents combusted, as above. The CO_2 was then transferred to another tube and graphitized as above. After graphitization, the sample was transferred into an aluminum sample holder (cathode) and pressed into a 0.040" diameter hole that was 0.040" deep. The sample holder was then placed into the PRIME Lab ion source (reference below) which typically generates ^{13}C-currents of 500-750 nA with the corresponding $^{14}C^{4+}$ ion detection rates of about 200 Hz for a sample ^{14}C-enrichment of about 2 x 10^{-12} of total carbon. The $^{14}C/^{12}C$ ratios were analyzed with no $\delta^{13}C$ correction. Standards of known ratio are constantly measured to normalize the values of the unknown. Samples were typically measured until they were used up or a precision of 1% was achieved.

Ion source reference (can be used for both the aluminum and carbon AMS part): G.S. Jackson, D. Elmore, M. Caffee, K.A. Mueller, B. De Bonte, P. Muzikar, B. Alexander, Nuclear Instruments and Methods in Physics Research Section B: Beam Interactions with Materials and Atoms 223-224 (2004) 155.

3. Results and Discussion

3.1 Particle size analysis

Figure 1 shows the morphology of neat nanoalumina. The top surfaces of most nanoalumina were square. It is not very easy to determine if they were cubic or square disks. The typical particle size was 50 to 80 nm. However, some smaller (30 nm) and larger particles (100 nm) existed, which may come from sintering and Ostwald ripening in the hydrothermal and calcination processes. Figure 2 shows the volume-averaged particle size distribution of neat and citrate-coated nanoalumina in their dispersion. The dispersion of neat nanoalumina showed three peaks: one centered at 95 nm (65 nm < D < 180 nm); one over the range, 230 nm to 500 nm; and one over the range, 1 μm to 2 μm. The peak centered at 95 nm was consistent with the size observed in SEM. The larger peaks likely represent agglomerates. The dispersion of citrate-coated nanoalumina showed only two peaks: one over the range of 65 to 105 nm with a peak at 83 nm and a second over the range, 230 to 360 nm. No larger agglomerates were observed. The results shows the citrate coating helped stabilize the dispersion of nanoalumina.

3.2 Thermogravimetric analysis of nanoalumina

Figure 3 shows the TGA curves of neat and citrate-coated nanoalumina. The weight of the neat nanoalumina decreased 0.68% due to the loss of surface hydroxyls. Based on a method to estimate surface density of functional groups [24], the sample had a surface density of 17 hydroxyl groups/nm^2, assuming an average particle was a 60 nm cube. For the citrate-coated nanoalumina, the weight loss was 3.85%. The 3.2% difference was attributed to decomposition of the citrate coating. The estimated surface density of citric acid is 3.3[Doesn't this need some unit?]/nm^2. Using a molecular diameter of citric acid of 0.57 nm [41], the coverage of citrate-coating was estimated to be 77% [42].

3.3 ^{26}Al in dosing material

Table 1 shows the ratio of $^{26}Al/^{27}Al$ obtained by AMS and the calculated fraction of ^{26}Al in samples. The $^{26}Al/^{27}Al$ ratio in dosing material sample Al_2O_3-1 was 1.41×10^{-9}. The number of ^{26}Al in Al_2O_3-1 was 1.26×10^{11} atoms. The $^{26}Al/^{27}Al$ ratio in Al_2O_3-2 was 1.20×10^{-9}. It contained 1.07×10^{11} ^{26}Al atoms. The

226 average number of ^{26}Al atoms in Al_2O_3-1 and Al_2O_3-2 was 1.16×10^{11}. Both of them were 10 µL aliquots
227 of 100-fold diluted dosing material. So the dosing material had an average number concentration of
228 1.16×10^{15} ^{26}Al /ml. The treated rat received 0.4 ml of the dosing material, corresponding to 4.65×10^{14} ^{26}Al
229 atoms or 0.383 nCi. It was 2.4 times the planned dose.

230 3.4 ^{26}Al in tissue samples

231 The $^{26}Al/^{27}Al$ ratio in liver-1 sample (38.7 mg) was 2.41×10^{-9}. The liver-1 sample contained 2.15×10^{11}
232 ^{26}Al atoms. The liver weight from dosed and control rats was around 16.3 grams so the total liver would
233 contain 9.06×10^{13} ^{26}Al atoms or 7.47×10^{-2} nCi, corresponding to 19.5% of the dose. The $^{26}Al/^{27}Al$ ratio in
234 liver-2 (35.9 mg) was 7.61×10^{-13}. The liver-2 sample contained 6.78×10^{7} ^{26}Al atoms so the total liver of
235 control rat would contain 3.08×10^{10} ^{26}Al atoms or 2.54×10^{-5} nCi, more than 3 orders of magnitude less
236 than the liver from the dosed rat. The weight of liver was about 3.2% of the rat's weight and contained
237 19.5% of dose, showing accumulation of the nanoalumina in the liver.

238 The $^{26}Al/^{27}Al$ ratio in the brain-1 sample was 5.99×10^{-11}. Brain-1 sample (757.1 mg) contained 5.35×10^{9}
239 ^{26}Al atoms. The average weight of a rat's brain is 1.86 gram so the total brain would contain 1.31
240 $\times10^{1026}Al$ atoms or 1.08×10^{-5} nCi, about 0.003% of the dosing material. The $^{26}Al/^{27}Al$ ratio in brain-2 was
241 5.01×10^{-11}. Brain-2 sample (738 mg) contained 4.47×10^{9} ^{26}Al atoms so the total brain from control rat
242 contained 1.13×10^{10} nCi ^{26}Al atoms or 9.27×10^{-6} nCi.

243 The $^{26}Al/^{27}Al$ background for samples without ^{26}Al was around 10^{-14} in the AMS measurements. So the
244 high $^{26}Al/^{27}Al$ ratio in the control rat suggests that some low-level contamination happened during
245 infusion or surgery. We can't compare the actual difference between the ^{26}Al in (brains?) from dosed and
246 control rats. However, the 0.003% of dosing material can be considered as the upper limit of ^{26}Al in the
247 brain from dosed rats. It indicates only a very small amount (if any) of the ^{26}Al got incorporated into the
248 brain since the nanoalumina did not cross the blood-brain barrier to enter brain parenchyma.

The $^{26}Al/^{27}Al$ ratio in bone-1 sample was 4.62×10^{-12}. The bone-1 tissue (52 mg) contained 4.12×10^{8} ^{26}Al atoms. The total rat skeletal weight is about of 5% of body weight (25 gram). So the total skeletal system would contain 1.98×10^{11} ^{26}Al atoms or 1.63×10^{-4} nCi, 0.043% of the dose. The bone-2 (50.8 mg) contained 7.52×10^{8} ^{26}Al atoms, translating to a total rat skeletal content of 3.05×10^{-4} nCi. The control rat bone had higher radioactivity in the bone than the dosed animal. The unexpected result may be from the same low level contamination that affected the brain. The 0.043% of dosing material was used as the upper limit and indicates only small amount (if any) of the ^{26}Al got incorporated into the brain. In the typical mammal, 60% of the body burden of Al is in the skeletal system and only 3% in the liver [43]. The high concentration of ^{26}Al in liver and low concentration in bone suggests that the ^{26}Al from the nanoalumina is difficult to dissolve and redistribute into bone.

3.5 ^{14}C in dosing material

Table 2 shows the ratio of $^{14}C/^{12}C$ obtained by AMS and the calculated sample activity. The $^{14}C/^{12}C$ in CA-1, CA-2, and CA-3 samples was 10353, 9342, and 8359, giving an average number of 1.1×10^{9} ^{14}C atoms in the three aliquots. They were 10 μL aliquots of 10-fold diluted dosing material so the dosing material had number concentration of 1.1×10^{12} ^{14}C atoms/mL. The rat got 0.4 mL of the dosing material, corresponding to 4.40×10^{11} ^{14}C atoms or 4.56×10^{-2} nCi. It was 28.5% of the planned dose.

3.6 ^{14}C in tissue samples

Because ^{14}C is ubiquitous in air, water and food, it inevitably enters the animal to become stored and form the ^{14}C background. The typical ratio $^{14}C/^{12}C$ of mammal's tissue sample via previous AMS measurements is around 1250. It is very close to a value reported in literature [44]. However, the precise ratio in each organ does vary, so we used the ratios in the control rat as our background.

After subtracting the average $^{14}C/^{12}C$ ratio background (1437.5) from Liver-2 and Liver-3 samples, the actual $^{14}C/^{12}C$ ratio in liver-1 sample was 607.5. The typical carbon percent in liver is 15 wt%. There are

1.23×10^{23} ^{12}C atoms in total liver (16.3 grams). The calculated ^{14}C in the total liver of the dosed rat was 7.45×10^{10} or 7.72×10^{-3} nCi, 16.9% of the dose. The ^{14}C of the coating material concentrated in the liver of the dosed rat, but the differences between the dosed rat and the controls was not as large as those for the core material, ^{26}Al.

The $^{14}C/^{12}C$ ratio (1261) from Brain-2 of the control rat was used as the background. After subtracting background, the $^{14}C/^{12}C$ in brain-1 sample is 22. The difference is larger than one standard deviation of the measured value so there was some higher amount of ^{14}C in brain of the dosed rat than the control rat in a statistically significant sense. The typical carbon percent in brain is 15 wt%. There are 1.40×10^{22} ^{12}C atoms in the total brain (1.86 grams). The total brain would contain 3.08×10^{8} ^{14}C atoms or 3.19×10^{-5} nCi, 0.07% of the dosage. For the Brain-3 sample, the $^{14}C/^{12}C$ ratio is much higher than brain-2 sample, even brain-1. The contamination may have come from a previous sample with high ratio of $^{14}C/^{12}C$ that was dried in the vacuum centrifuge. This seemed highly likely since a check of the records at the PRIME Lab showed that the one sample was dried with a batch of samples that had $^{14}C/^{12}C$ ratios 100 times higher. Thus, it was considered safe to discard this result.

After subtracting the average $^{14}C/^{12}C$ ratio background (1412.5) from Bone-2 and Bone-3 samples, the actual ratio of $^{14}C/^{12}C$ in bone-1 sample was 76.5. The typical carbon percent in bone was around 12% [45]. There are 1.51×10^{23} ^{12}C atoms in total bone (25 grams). The total bone would contain 1.16×10^{10} ^{14}C atoms or 1.20×10^{-3} nCi, 2.63% of the dosage. The bone from the dosed rat had higher ^{14}C than that from the control rat.

3.7 The ratio of coating/core and material balance

The ratio between $^{14}C/^{26}Al$ in different organs and the mass distribution are shown in Table 3. In the dosing material, the average numbers of ^{26}Al and ^{14}C atoms were 4.65×10^{14} and 4.40×10^{11} respectively.

The $^{14}C/^{26}Al$ was 9.46×10^{-4}. The total recovered ^{26}Al and ^{14}C from liver, brain and bone are 19.5% and 19.6% of the dosing material respectively.

The numbers of isotope atoms in the dosed liver were: $^{26}Al = 9.06\times10^{13}$ and $^{14}C = 7.45\times10^{10}$. The $^{14}C/^{26}Al$ in liver of the dosed rat was 8.22×10^{-4}, around 87% of the ratio in the dosing material. The citrated coating entering the liver (19.5% of dosage) partially dissociated from the nanoalumina, and would have been available to redistribute into organs such as the brain and bone.

The average numbers of isotope atoms in brain were: $^{26}Al < 1.31\times10^{10}$ and $^{14}C = 3.08\times10^{8}$, for a $^{14}C/^{26}Al$ ratio $> 2.35\times10^{-2}$. The average numbers of isotope atoms in bone were: $^{26}Al < 1.98\times10^{11}$ and $^{14}C = 1.16\times10^{10}$, for a $^{14}C/^{26}Al$ calculated ratio $> 5.81\times10^{-2}$. Both of these ratios are much higher than that of the dosing material. The reason is that ^{14}C preferentially accumulated in brain (0.07%) and bone (2.63%) compared to the levels of ^{26}Al in these two organs (0.003% and 0.043%, respectively). This finding suggests that some of the citrate coating dissociated from the nanoalumina's surface and then redistributed to organs such as the brain and bone.

4. Conclusions

The core and surface coatings of a complex engineered nanoparticle have been tracked during biological exposure to the rat using rare isotope labels detected by AMS. The alumina core was tracked using ^{26}Al and the citrate coating was tracked using ^{14}C. Comparison of the rare isotope levels and their ratios, ^{14}C:^{26}Al, in different organs demonstrated the relative stability of the two CENP components. The amount of ^{26}Al in the liver of the dosed rat was higher than that of control rats. The amounts of ^{26}Al in brain and bone of the dosed rat were similar to those of the control rat. It suggests the nanoalumina accumulated, and persisted in the liver 30 days after infusion. The amounts of ^{14}C in the liver, bone, and brain of the dosed rat were also higher than those of the control rats. However, the $^{14}C/^{26}Al$ ratios differed between

liver, brain, and bone. Slightly less coating material went to the liver compared to the core material and its levels were significantly higher in brain and bone compared to the core material. Some of the citrate coating dissociated from the nanoparticle surfaces and redistributed to organs such as the brain and bone. AMS methodology provides a new opportunity to characterize the biodistribution of complex engineering nanomaterials.

5. Acknowledgement

This work was supported by National Science Foundation to **"**EAGER: Low-level detection of complex nanomaterials in biological media" **[**Award Abstract #1249123**]**. Although the research described in this article has been funded wholly or in part by the National Science Foundation, it has not been subjected to the Agency's required peer and policy review and therefore does not necessarily reflect the views of the National Science Foundation and no official endorsement should be inferred.

References

[1] A. Verma, V.M. Rotello, Chem. Commun., (2005) 303-312.
[2] M. De, S. Rana, H. Akpinar, O.R. Miranda, R.R. Arvizo, U.H.F. Bunz, V.M. Rotello, Nat. Chem, 1 (2009) 461-465.
[3] A.M. Smith, H.W. Duan, A.M. Mohs, S.M. Nie, Adv. Drug Delivery Rev, 60 (2008) 1226-1240.
[4] M.E. Davis, Z. Chen, D.M. Shin, Nat. Rev. Drug Discovery, 7 (2008) 771-782.
[5] M. Pailleux, D. Boudard, J. Pourchez, V. Forest, P. Grosseau, M. Cottier, Toxicology In Vitro, 27 (2013) 1049-1056.
[6] R.A. Yokel, M.T. Tseng, M. Dan, J.M. Unrine, U.M. Graham, P. Wu, E.A. Grulke, Nanomedicine (New York, NY, United States), 9 (2013) 398-407.
[7] X. Huang, B. Wang, E.A. Grulke, M.J. Beck, Journal of Chemical Physics, 140 (2014) 074703/074701-074703/074709.
[8] K. Hund-Rinke, T. Klawonn, in, Fraunhofer Institute for Molecular Biology and Applied Ecology IME, Schmallenberg, Germany., 2013, pp. F/1-F/3, i-xxv, 1-431.
[9] K. Smits, J. Liepins, M. Gavare, A. Patmalnieks, A. Gruduls, D. Jankovica, IOP Conference Series: Materials Science and Engineering, 38 (2012) 012050/012051-012050/012054.
[10] L.Q. Chen, P.P. Hu, L. Zhang, S.Z. Huang, L.F. Luo, C.Z. Huang, Science China: Chemistry, 55 (2012) 2209-2216.
[11] V. Kanniah, B. Wang, Y. Yang, E.A. Grulke, Journal of Applied Polymer Science, (2012) Ahead of Print.
[12] H. Jin, D.A. Heller, M.S. Strano, Nano Letters, 8 (2008) 1577-1585.
[13] L.M. Bimbo, L. Peltonen, J. Hirvonen, H.A. Santos, Current Drug Metabolism, 13 (2012) 1068-1086.
[14] E. Parliament, P.D.E.a.S. Policy, in, 2006.

[15] J. Ai, E. Biazar, M. Jafarpour, M. Montazeri, A. Majdi, S. Aminifard, M. Zafari, H.R. Akbari, H.G. Rad, International Journal of Nanomedicine, 6 (2011) 1117-1127.
[16] Z. Li, Y. Geng, X. Zhang, W. Qi, Q. Fan, Y. Li, Z. Jiao, J. Wang, Y. Tang, X. Duan, W. Wu, J. Nanopart. Res., 13 (2011) 2939-2947.
[17] R.A. Yokel, T.C. Au, R. MacPhail, S.S. Hardas, D.A. Butterfield, R. Sultana, M. Goodman, M.T. Tseng, M. Dan, H. Haghnazar, J.M. Unrine, U.M. Graham, P. Wu, E.A. Grulke, Toxicological Sciences, 127 (2012) 256-268.
[18] I. Lynch, K.A. Dawson, Nano Today, 3 (2008) 40-47.
[19] T. Cedervall, I. Lynch, S. Lindman, T. Berggard, E. Thulin, H. Nilsson, K.A. Dawson, S. Linse, Proceedings of the National Academy of Sciences of the United States of America, 104 (2007) 2050-2055.
[20] R. Yokel, Grulke, E., MacPhail, R. Metal-based nanoparticle interactions with the nervous system: the challenge of brain entry and the risk of retention in the organism, WIREs Nanomed Nanobiotechnol, 5 (2013) 346-373.
[21] T.M. Dan M, Wu P, Unrine JM, Grulke EA, Yokel RA., Int J Nanomedicine, 7 (2012) 4023-4036.
[22] A.B. Al Faraj, Amine; Cieslar, Katarzyna; Lacroix, Ghislaine; Canet-Soulas, Emmanuelle; Cremillieux, Yannick, nanotechnology, 21 (2010) 175103/175101-175103/175109.
[23] Y.Y. Tsutsumi, Yasuo, Nature Nanotechnology, 6 (2011).
[24] V.W. Kanniah, Binghui; Yang, Ying; Grulke, Eric A, Journal of Applied Polymer Science, 125 (2012) 165-174.
[25] C. Perez-Campana, V. Gomez-Vallejo, M. Puigivila, A. Martin, T. Calvo-Fernandez, S.E. Moya, R. Ziolo, T. F.Reese, J. Llop, ACS NANO, 7 (2013) 3498-3505.
[26] S. Rojas, J.D. Gispert, S. Abad, M. Buaki-Sogo, V.M. Victor, H. Garcia, J.R. Herance, Mol. Pharmaceutics, 9 (2012) 3543-3550.
[27] K. Brown, E.M. Tompkins, I.N.H. White, Mass Spectrometry Reviews, 25 (2006) 127-145.
[28] M. Larsson, Mass Spectrometry Reviews, 27 (2008) 398-427.
[29] J. Barker, R.C. Garner, Rapid communications in mass spectrometry : RCM, 13 (1999) 285-293.
[30] T.J. Ognibene, J.S. Vogel, Synthesis and Applications of Isotopically Labelled Compounds, Proceedings of the International Symposium, 8th, Boston, MA, United States, June 1-5, 2003, (2004) 293-295.
[31] M. Gaskell, R. Jukes, D.J.L. Jones, E.A. Martin, P.B. Farmer, Chemical Research in Toxicology, 15 (2002) 1088-1095.
[32] J.S. Vogel, Nuclear Instruments & Methods in Physics Research, Section B: Beam Interactions with Materials and Atoms, 172 (2000) 884-891.
[33] N.D. Priest, Journal of environmental monitoring : JEM, 6 (2004) 375-403.
[34] R. Peteranderl, C. Lechene, Journal of the American Society for Mass Spectrometry, 15 (2004) 478-485.
[35] G.K. Chuah, S. Jaenicke, T.H. Xu, Microporous and Mesoporous Materials, 37 (2000) 345-353.
[36] H.K. Farag, F. Endres, Journal of Materials Chemistry, 18 (2008) 442-449.
[37] M.M.a.D.A.A.-S. Barbooti, Thermochimica Acta, 98 (1986) 119-126.
[38] R.A. Yokel, J.M. Melograna, Biological Trace Element Research, 5 (1983) 225-237.
[39] R.D. Brauer, J.D. Robertson, P. Sharma, R.A. Yokel, Nuclear Instruments & Methods in Physics Research, Section B: Beam Interactions with Materials and Atoms, 152 (1999) 129-134.
[40] G.B. T.J. Ognibene, J.S. Vogel, G.F. Peaslee, S. Murov, Anal. Chem., 75 (2003) 2192-2196.
[41] M.A. van Drunen, R. Finsy, H.G. Merkus, B. Scarlett, G.M. van Rosmalen, Journal of Crystal Growth, 134 (1993) 196-202.
[42] B.W. Wang, Peng; Yokel, Robert A.; Grulke, Eric A., Applied Surface Science, 258 (2012) 5232-5241.
[43] D. Krewski, R.A. Yokel, E. Nieboer, D. Borchelt, J. Cohen, J. Harry, S. Kacew, J. Lindsay, A.M. Mahfouz, V. Rondeau, Journal of Toxicology and Environmental Health, Part B: Critical Reviews, 10, Suppl 1 (2007) 1-269.
[44] J. Sabol, P.-s. Weng, Introduction to Radiation Protection Dosimetry, World Scientific, 1995.
[45] R.L. Mehta, Ryan A.; Fitch, Hannah M.; Ali, Nawab; Soulsby, Michael; Chowdhury, Parimal, AIP Conference Proceedings, 1099 (2009) 259-264.

Figure 1.

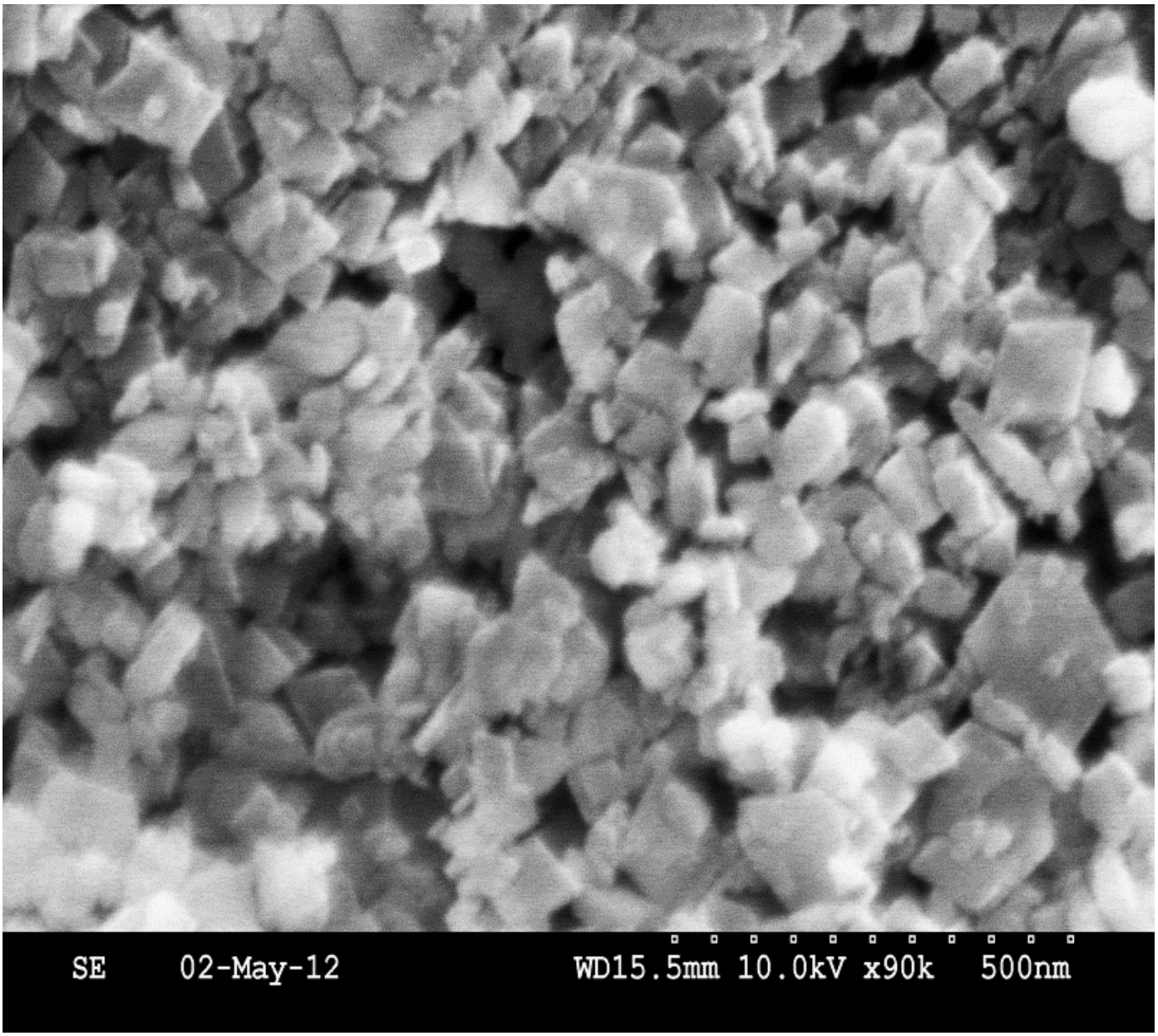

Figure 2.

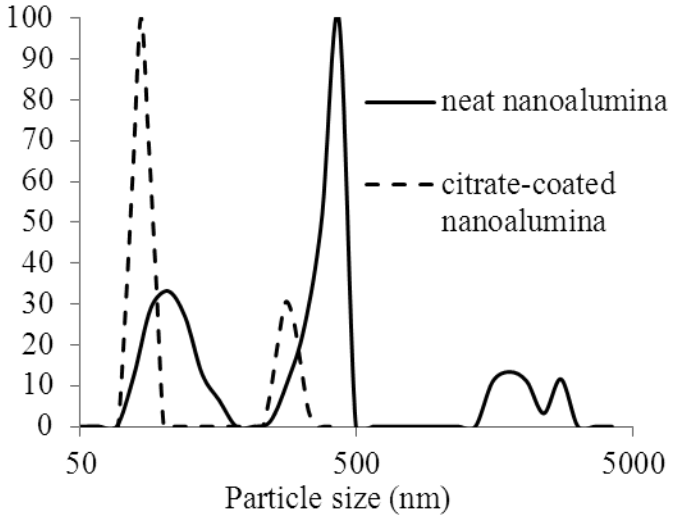
100
90
80
70
60
50
40
30
20
10
0
50
500
5000
Particle size (nm)
neat nanoalumina
citrate-coated nanoalumina

405 Figure 3.

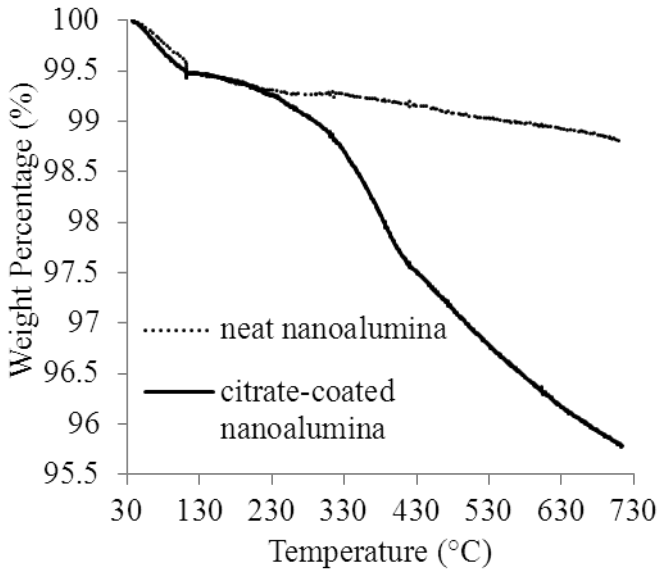

406